Full-torus Impurity Transport Simulation for Optimizing Plasma Discharge Operation Using a Multi-species Impurity Powder Dropper in the Large Helical Device

M. Shoji[1*], **G. Kawamura**[1,2], **R. Smirnov**[3], **Y. Tanaka**[4], **S. Masuzaki**[1], **Y. Uesugi**[4], **N. Ashikawa**[1,2], **E. Gilson**[5], **and R. Lunsford**[5]

[1] National Institute for Fusion Science, National Institutes of Natural Sciences, Oroshi-cho, Toki, Gifu 509-5292 Japan

[2] Graduate University for Advanced Studies (SOKENDAI), Oroshi-cho, Toki, Gifu 509-5292 Japan
[3] University of California at San Diego, La Jolla, CA 92093 USA
[4] Kanazawa University, Kakuma, Kanazawa 920-1192 Japan
[5] Princeton Plasma Physics Laboratory, 100 Stellarator Rd, PO Box 241, Princeton, NJ 08543 USA

Received XXXX, revised XXXX, accepted XXXX
Published online XXXX

Key words impurity powder dropper, DUSTT, EMC3-EIRENE, ergodic layer, LHD

The transport of impurities supplied by a multi-species impurity powder dropper (IPD) in the Large Helical Device (LHD) is investigated using a three-dimensional peripheral plasma fluid code (EMC3-EIRENE) coupled with a dust transport simulation code (DUSTT). The trajectories of impurity powder particles (Boron, Carbon, Iron and Tungsten) dropped from the IPD and the impurity transport in the peripheral plasma are studied in a full-torus geometry. The simulation reveals an appropriate size of the impurity powder particles and an optimum operational range of the dust drop rates for investigating the impurity transport without inducing radiation collapse. The simulation also predicts a favorable plasma discharge condition for wall-conditioning (boronization) using the IPD in order to deposit boron to high plasma flux and neutral particle density areas in the divertor region in the inboard side of the torus.

1 Introduction

Impurity powder injection has been expected to be an attractive optional technique for impurity seeding for investigating impurity ion transport, wall conditioning, and dust dynamics studies in magnetic plasma confinement devices [1, 2]. A multi-species impurity powder dropper (IPD) is planned to be installed in the Large Helical Device (LHD) from the next experimental campaign. The LHD consists of superconducting helical and poloidal coils for forming plasma confinement magnetic field configurations without the toroidal plasma current [3]. The non-axisymmetric magnetic field components produced by the helical coils intrinsically form ergodized magnetic field line structures (ergodic layer) around the main plasma confinement region. The magnetic field lines are bundled into four divertor legs which deviate from the outermost surface of the ergodic layer [4]. On applying the IPD to the plasma discharge experiments, there is a concern that the dropped impurity powder particles (dust) cannot reach the ergodic layer because of the effect of the plasma flow in the divertor legs which can perturb the original free-fall trajectories of the dust particles [5]. The trajectories are investigated using a three-dimensional peripheral plasma fluid code (EMC3-EIRENE) [6-8] coupled with a dust transport simulation code (DUSTT) [9-11] in the LHD full-torus geometry. The simulation codes are powerful tools for predicting the falling trajectories of the impurity dust particles, impurity ion transport in the peripheral plasma, and the impurity ion flux distribution on the vacuum vessel and the divertor plates. The simulation is expected to reveal an optimum operational condition for applying the IPD to study the impurity transport in the ergodic layer without inducing radiation collapse and to perform an effective wall-conditioning (boronization) during main plasma discharges.

This paper describes the simulation results of the trajectories of four kinds of impurity dust particles (Boron, Carbon, Iron, and Tungsten) in order to find an appropriate experimental condition for the IPD. The simulation also predicts an operational range of the drop rate of the impurity dust for investigating the impurity transport. In the last section, toroidal and poloidal distribution of the boron ion flux density is calculated in the full-torus geometry in order to find an optimum plasma regime for the wall conditioning using the IPD.

* Corresponding author. E-mail: shohji.mamoru@nifs.ac.jp, Phone: +81 572 58 2151, Fax: +81 572 58 2618

2 Simulation of the trajectories of impurity dust particles

A three-dimensional model for the simulation for tracking the impurity dust particles is illustrated in Figure 1, which is for the most typical magnetic configuration where the radial position of the magnetic axis R_{ax} locates at 3.60 m. The model includes the peripheral plasma (the ergodic layer and the divertor legs), the vacuum vessel, the helical coil cans, and the divertor plates for one-half of the helical coil pitch angle (18˚ in toroidal direction) [12]. A poloidal cross-section of a typical plasma density profile in the peripheral plasma at the toroidal angle where the IPD is installed is also shown in this figure. Plasma parameter profiles (deuterium plasma density, ion and electron temperature, and the plasma flow velocity) are obtained by fitting simulation results to measured electron density and temperature profiles, in which the perpendicular particle and the thermal diffusion coefficients in the plasma are set to 0.5 and 1.5 m^2/s, respectively. The EMC3-EIRENE code provides the density profile of the impurity ions in the peripheral plasma by solving the continuity and the momentum balance equations of the impurity ions for each ionization stage. The ionization/recombination coefficients of the impurity ions and the radiation power are derived from database on the Atomic Data and Analysis Structure (ADAS) [13]. A converged solution of plasma parameter profiles is obtained by an iterative calculation scheme in the simulation code. The input parameters for the simulation are the plasma heating power and the plasma density at the Last Closed Flux Surface (LCFS) (P^{LCFS} and n_e^{LCFS}).

The initial position of the impurity dust particles is placed at an upper part in the vacuum vessel as shown in a yellow circle in Figure 1. The dust particles are dropped from this position in free fall at an initial velocity (v_{dust}) of 5.0 m/s corresponding to the speed in which the dust particles are dropped from the actual installed position of the IPD on an upper port (outside of this model). The trajectories of the dust particles are simulated using the DUSTT on the background plasma parameters calculated by the EMC3-EIRENE. In the DUSTT, it is assumed that the shape of the dust particles is spherical and the dust consists of a single element. This code provides the three-dimensional profile of the production rate of the neutral impurity atoms originated from the dust particles evaporated/sublimated by the plasma heat load. The simulation adopts the assumption that all the neutral impurity atoms are immediately ionized at the positions of their production in the plasma. For simplicity, impurities produced by sputtering processes on the surface of the vacuum vessel and the divertor plates are not included.

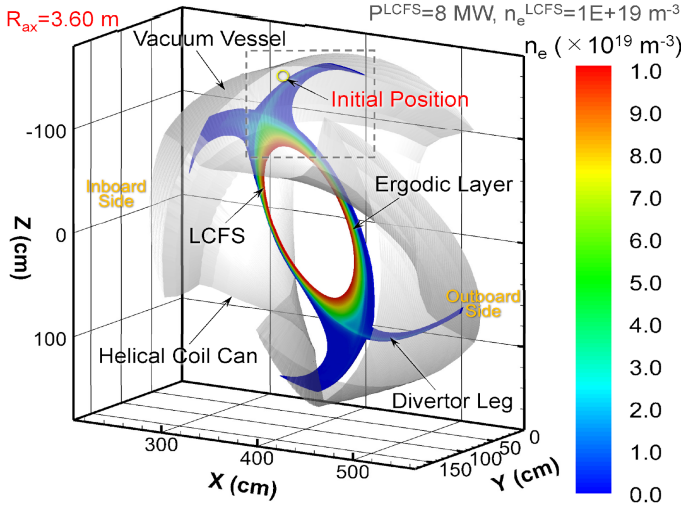

Fig. 1 A three-dimensional model for impurity transport simulation using the EMC3-EIRENE coupled with the DUSTT for the standard magnetic configuration (R_{ax}=3.60 m) with a poloidal cross section of the typical plasma density profile. A dark grey broken square corresponds to the area of the enlarged view shown in Figure 2.

Enlarged views showing the trajectories of boron, carbon, iron, and tungsten dust particles dropped from the initial position are presented in figure 2 (a-d), respectively, in which the diameter of the dust (d_{dust}) is varied from 10 μm to 200 μm for low and high plasma density conditions (n_e^{LCFS}=1×10^{19} m^{-3} and 4×10^{19} m^{-3} with P^{LCFS} =8 MW). The effect of the magnetization of the iron dust is not included. The dust particles cross an upper divertor leg before reaching the ergodic layer. The trajectories of the dust particles having a smaller specific gravity like boron and carbon are deviated from the original free fall trajectories. The trajectories of small sized dust particles (d_{dust}≤20 μm) are also have a tendency to be bent at the divertor leg, which is caused by the effect of the ion drag force due to the plasma flow in the divertor leg. The deviation of the trajectories is more striking in the high

plasma density case as depicted as colored broken lines in these figures. These lighter and smaller dust particles collide with the surface on the helical coil can or the vacuum vessel in the end. The positions where the dropped dust particles are completely evaporated or sublimated are marked with small colored circles, showing that larger and heavier dust particles deeply penetrate into the ergodic layer nearby the LCFS (Small circles outside of the plasma indicate the evaporation or sublimation positions at a toroidal angle being far away from the IPD position.). This simulation proves that the largest sized dust particles (d_{dust}=200 μm) for the lower plasma density are favorable for depositing the impurity sources in the peripheral plasma (ergodic layer) in all four impurity dust particle cases.

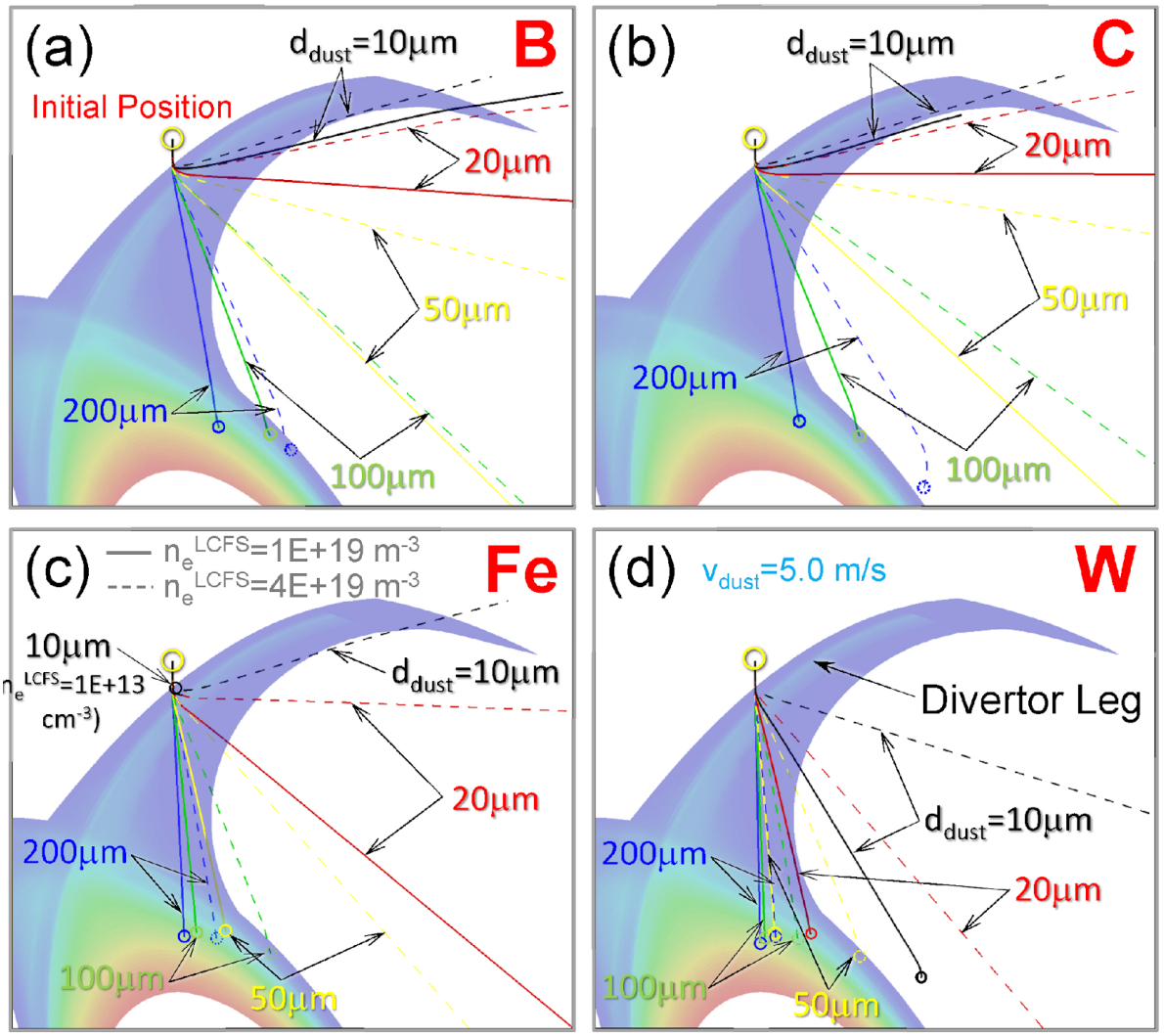

Fig. 2 An enlarged view showing the trajectories of dropped boron, carbon, iron, and tungsten dust with various dust sizes d_{dust} in the range from 10 μm to 200 μm for low and high plasma density conditions (n_e^{LCFS}=1×10^{19} m^{-3} and 4×10^{19} m^{-3} with P^{LCFS} =8 MW). The trajectories for the low and high plasma densities are depicted as solid and broken lines, respectively. Small circles indicate the positions where the dropped dust particles are completely evaporated or sublimated in the plasma.

3 Operational range of the drop rate of impurity dust particles

The deposited impurities in the ergodic layer enhance the impurity radiation power (P_{imp}) and decrease the average divertor plasma temperature (T_e^{div}). It is experimentally found that excessive impurity ions in the plasma leads to radiation collapse and terminates the plasma discharges [14]. In order to find an optimum drop rate of the impurity powder particles, the dependence of the impurity radiation power and the divertor plasma temperature on the drop rate is investigated using the simulation code for four impurity particles (Boron, Carbon, Iron, and Tungsten with d_{dust}=200 μm). The three-dimensional model for one-half of the helical coil pitch angle is used in order to obtain a converged solution by the iterative calculation between the two codes (the EMC3-EIRENE and the DUSTT) within reasonable CPU time. The maximum number of impurity dust particles

for tracking the trajectories in this simulation is two million. Figure 3 shows the dependence of the two parameters (P_{imp} and T_e^{div}) on the dust drop rate for the four impurities. The drop rate (horizontal axis) corresponds to the number of the impurity atoms dropped by the IPD per one second for the full-torus geometry. The impurity radiation power (vertical axis) is also equivalent to the power for the full torus. The maximum value of the vertical axis equals to the total plasma heating power at the LCFS (the power source for the peripheral plasma) in this simulation. The diameter of dust particles and the initial drop speed are set to 200 μm and 5 m/s, respectively. The input parameters are fixed to those for the low plasma density condition (P^{LCFS} =8 MW and n_e^{LCFS}=1×10^{19} m^{-3}). Figure 3 indicates that while the impurity radiation power increases with the dust drop rate, the divertor plasma temperature decreases with the drop rate. Converged solutions are not obtained when the divertor plasma temperature becomes less than about 17 eV. The simulation results provide an appropriate operational range of the drop rate without inducing the radiation collapse. The heavier impurity (Iron and Tungsten) dust particles drastically enhance the radiation power at relatively lower drop rates of around 1×10^{21} and 3×10^{20} atom/s, respectively. For the lighter impurity (Boron and Carbon) dust particles, the radiation power significantly rises at a higher drop rate of around 1×10^{22} atom/s, indicating that the plasma is sustained at higher drop rates in the case of the lighter impurities. These simulation results are explained by the high radiation power by heavier impurity ions and the deep penetration of the heavier impurity dust particles into the ergodic layer as shown in Figure 2. The simulation reveals the appropriate range of the dust drop rates for investigating impurity transport for the four impurity dust particles. For example, in the boron dust case, the optimum drop rate is less than about 1×10^{22} atom/s in which the impurity radiation power in the peripheral plasma is less than 20 % of the total plasma heating power (P^{LCFS}) being less than the radiation power which can trigger the radiation collapse in this case.

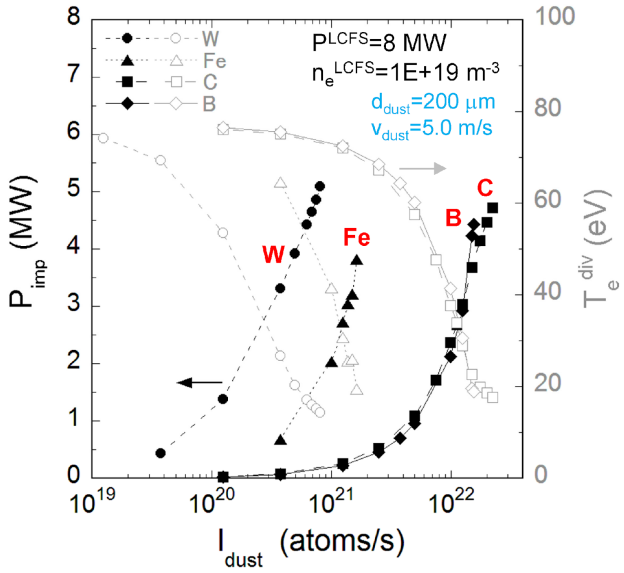

Fig. 3 The dependence of the impurity radiation power P_{imp} and the divertor electron temperature T_e^{div} on the drop rate of (a) Boron, (b) Carbon, (c) Iron, and (d) Tungsten dust particles I_{dust}.

4 Full-torus simulation of boron ion transport for wall conditioning

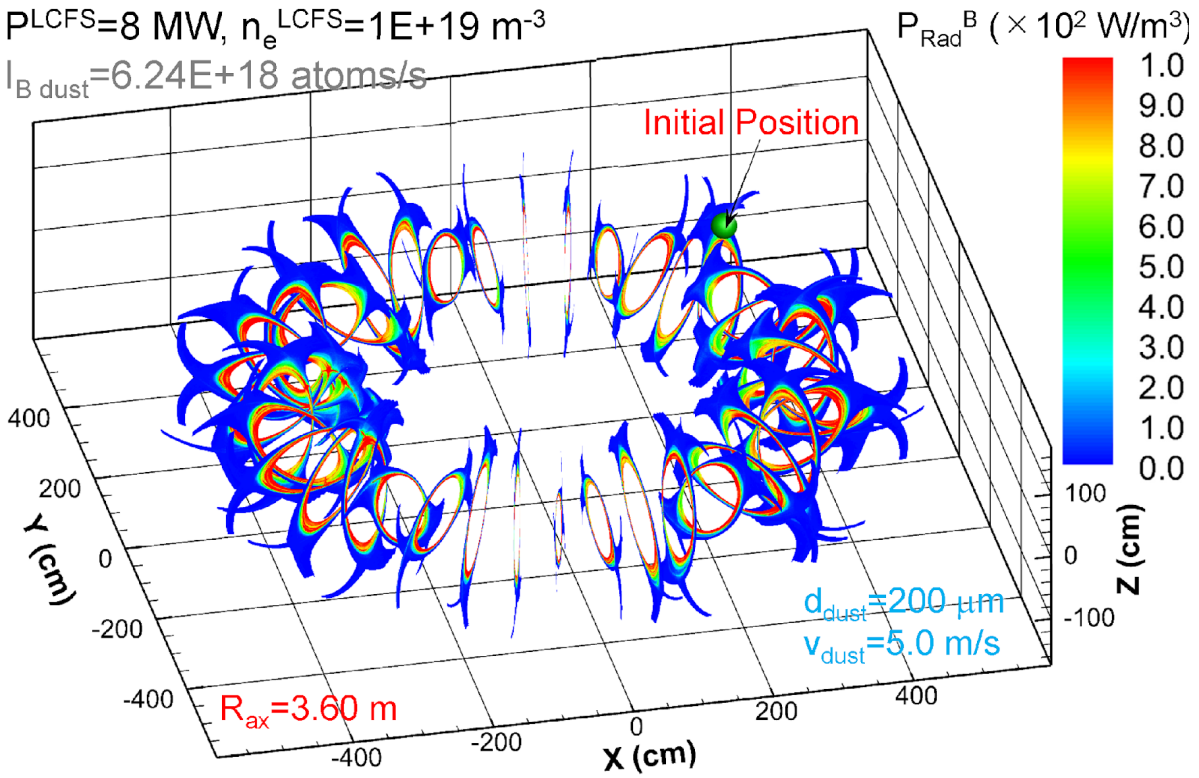

Fig. 4 The full-torus profile of the poloidal cross sections of the radiation power density by the boron ions including all ionization stages originated from the boron dust particles supplied by the IPD in the peripheral plasma for the low plasma density (P^{LCFS}=8 MW and n_e^{LCFS}=1×10^{19} m^{-3}).

One of the main purposes of the IPD is real time wall conditioning by suppling boron powder particles during plasma discharges. For exploring the possibility of the IPD as a wall conditioning technique, full-torus boron ion transport simulation was carried out. In this simulation, for the first step, a background plasma parameter profile without born dust particles (d_{dust}=200 μm) is calculated in the three-dimensional model for one-half of the helical coil pitch angle in advance. For the next step, the background plasma parameter profile is expanded to the full-torus geometry with taking the upper/lower and helical symmetries in the model into account. For the last step, boron dust particles are dropped from the initial position in a model for the full-torus geometry with a very low dust drop rate of 6.24×10^{18} atoms/s which does not perturb the background plasma parameter profiles as demonstrated in Figure 3 (indicated as closed and open diamonds in Boron case). Figure 4 displays the full-torus profiles (the poloidal cross-sections at every 9° in the toroidal direction) of the radiation power density originated from the total boron ions with all ionization stages (P_{Rad}^{B}) in the peripheral plasma for the low plasma density condition (P^{LCFS} =8 MW and n_e^{LCFS}=1×10^{19} m^{-3}). The simulation shows that the radiation power is high near the LCFS which is explained by the formation of the thermal force dominant areas in the ergodic layer, which convey the impurity ions to the main plasma confinement region along the magnetic field lines in this case [15].

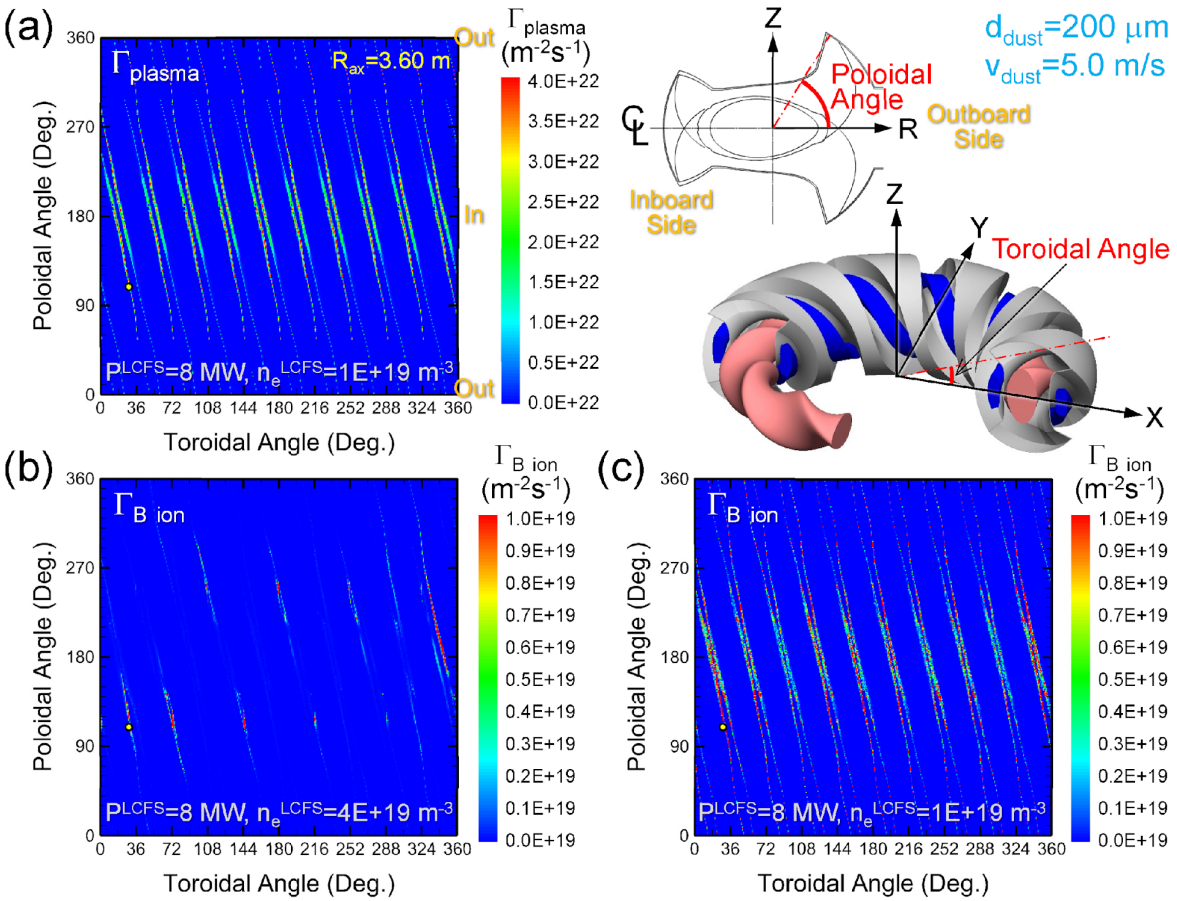

Fig. 5 (a) The toroidal and poloidal expansion of the plasma flux density distribution on the divertor plates and the vacuum vessel for R_{ax}=3.60 m. (b) The expansion of the boron ion flux density in a high plasma density condition (P^{LCFS} =8 MW and n_e^{LCFS}=4×10^{19} m^{-3}). (c) The expansion of the boron ion flux density for a low plasma density (n_e^{LCFS}=1×10^{19} m^{-3}). The initial position is indicated as a small yellow circle (the toroidal and poloidal angles are 30° and 109°, respectively.).

One of the critical issues for applying the IPD to the wall conditioning in non-axisymmetric and three-dimensionally complicated configuration like LHD is the delivering of boron to the divertor regions which locate in narrow and recessed areas between the two helical coil cans, where boron is hard to reach by standard glow discharges [16]. The simulation codes can calculate the full-torus distribution of the plasma (deuterium ion) and the boron ion flux density reaching the divertor plates and the vacuum vessel. Figure 5(a) gives the full-torus toroidal and poloidal expansion of the plasma flux density Γ_{Plasma} distribution for the standard magnetic configuration (R_{ax}=3.60 m), in which the plasma flux density is distributed along the four lines of the strike points where the four divertor legs intersect the divertor plates or the vacuum vessel. The flux density is significantly higher in the inboard side of the torus at the toroidal angles where the LHD plasma is horizontally elongated (around 180° in the poloidal angle). This trend has been experimentally confirmed by measurements with electrostatic probes and thermocouples embedded in divertor plates [16]. Figure 5(b) and (c) illustrate the figures of the full-torus toroidal and poloidal expansion of the distribution of the total boron ion flux density in high (n_e^{LCFS}=4×10^{19} m^{-3}) and low plasma density (n_e^{LCFS}=1×10^{19} m^{-3}) cases, respectively. The simulations in both of the two plasma density cases indicate that while the toroidal and poloidal distribution of the boron ion flux ($\Gamma_{B\ ion}$) for the high plasma density is more irregular as compared to the plasma flux distribution (Figure 5(a)), the distribution of $\Gamma_{B\ ion}$ for the low plasma density almost corresponds to the plasma flux distribution. It seems that the higher boron ion flux density in the inboard side of the torus is advantageous for the wall conditioning because the presence of the boron around this region can effectively contribute to the reduction of impurities because the plasma flux and neutral particle density is highly localized in this region for R_{ax}=3.60 m [17, 18]. One of the reasons for the disadvantageous distribution of the boron ion flux density in the high plasma density condition is attributed to the shallow penetration of boron dust particles into the ergodic layer as shown in Figure 2(a). This is caused by the deviation from the free-fall trajectories due to the higher ion drag force in the divertor legs. In addition to this, the boron ions originated from the dust particles are produced in an ion drag force dominant area at the outermost surface in the ergodic layer, where the impurity ions are exhausted to the

divertor plates along the plasma flow [19]. The impurity transport simulation in the full-torus geometry successfully found an appropriate operational condition of the LHD plasma discharge for effective wall conditioning using the IPD.

5 Summary

An appropriate operational condition of plasma discharges for a multi-species impurity powder dropper (IPD) was investigated using the EMC3-EIRENE coupled with the DUSTT. The simulation shows that the trajectories of the impurity dust particles having a smaller specific gravity such as Boron and Carbon are subjected to be bent by the effect of the plasma flow in the diverter leg. The trajectories of small sized dust particles ($d_{dust} \leq 20$ μm) are also deviated from the original free-fall trajectories, which prevents the impurity dust particles from reaching the ergodic layer and deep penetration of the dust particles into the ergodic layer. The deviation of the trajectories is more striking in the high plasma density case. The deviation of the trajectories is found to be striking in the high plasma density case. These simulation results demonstrate that the drop of large sized dust particles in lower plasma densities is favorable for the impurity transport study using the IPD. The analysis of the dependence of the impurity radiation power on the dust drop rate clarifies the optimum operational range of the drop rate without inducing the radiation collapse. The simulations in the full-torus geometry successfully found an appropriate plasma discharge condition for effectively delivering boron ions by the IPD to the inboard side of the torus where the plasma flux and neutral particle density is significantly high for the standard magnetic configuration in LHD.

Acknowledgments This work is performed under the auspices of the NIFS Collaboration Research program (NIFS12KNXN236). The author would like to thank Y. Feng for permission to use the EMC3-EIRENE. He is also grateful for the computational resources of the LHD numerical analysis server and the plasma simulator in NIFS. This work is also supported by JSPS KAKENHI Grant Numbers 16H04619, 16K18340, and the U.S. DOE Grant DE-FG02-06ER54852.

References

[1] A. Bortolon et al., Nuclear Materials and Energy **19**, 384 (2019).
[2] A. Nagy et al., Rev. Sci. Instrum. **89**, 10K121 (2018).
[3] Y. Takeiri et al., Nucl. Fusion **57**, 102023 (2017).
[4] N. Ohyabu et al., Nucl. Fusion **34**, 387 (1994).
[5] M. Shoji et al., Nuclear Materials and Energy **12**, 779 (2017).
[6] Y. Feng et al., Plasma Phys. Control. Fusion **44**, 611 (2002).
[7] G. Kawamura et al., Contrib. Plasma Phys. **54**, 437 (2014).
[8] G. Kawamura et al., Plasma Phys. Control. Fusion **60**, 084005 (2018).
[9] A. Yu Pigarov et al., J. Nucl. Mater. **363-365**, 216 (2007).
[10] R. D. Smirnov et al., Plasma Phys. Control Fusion **49**, 347 (2007).
[11] Y. Tanaka et al., J. Nucl. Mater. **415**, S1106 (2011).
[12] M. Shoji et al., Nuclear Materials and Energy **17**, 188 (2018).
[13] The ADAS User Manual (version 2.6) http://adas.phys.strath.ac.uk/ (2004).
[14] B. J. Peterson et al., Phys. Plasmas. **8**, 3861 (2001).
[15] M. Shoji et al., Contrib. Plasma Phys. **58**, 616 (2017).
[16] U. Schneider et al., J. Nucl. Mater. **176&177**, 350 (1990).
[17] S. Masuzaki et al., Nucl. Fusion **42**, 750 (2002).
[18] S. Masuzaki et al., Plasma Fusion Res. **6**, 1202007 (2011).
[19] M. Kobayashi et al., Contrib. Plasma Phys. **48**, 255 (2008).